Nuclear Engineering and Technology 53 (2021) 3816–3823

Contents lists available at ScienceDirect

Nuclear Engineering and Technology

journal homepage: www.elsevier.com/locate/net

Original Article

The influence of BaO on the mechanical and gamma / fast neutron shielding properties of lead phosphate glasses

K.A. Mahmoud [a, b, *], F.I. El-Agawany [c], O.L. Tashlykov [a], Emad M. Ahmed [d], Y.S. Rammah [c]

[a] Department of Nuclear Power Plants and Renewable Energy Sources, Ural Power Engineering Institute, Ural Federal University, 5 Sofia Kovalevskaya St., Yekaterinburg, Russia
[b] Nuclear Materials Authority, P. O. Box 530, El Maadi, Cairo, Egypt
[c] Menoufia University, Faculty of Science, Physics Department, 32511, Shebin El Koom, Egypt
[d] Department of Physics, College of Science, Taif University, PO Box 11099, Taif, 21944, Saudi Arabia

ARTICLE INFO

Article history:
Received 20 August 2020
Received in revised form
25 April 2021
Accepted 5 June 2021
Available online 18 June 2021

Keywords:
Mechanical properties
Gamma
Shield
Monte Carlo simulation code
Neutron

ABSTRACT

The mechanical features evaluated theoretically using Makishima-Mackenzie's model for glasses xBaO-(50-x) PbO−50P_2O_5 where x = 0, 5, 10, 15, 20, 30, 40, and 50 mol%. Wherefore, the elastic characteristics; Young's, bulk, shear, and longitudinal modulus calculated. The obtained result showed an increase in the calculated values of elastic moduli with the replacement of the PbO by BaO contents. Moreover, the Poisson ratio, micro-hardness, and the softening temperature calculated for the investigated glasses. Besides, gamma and neutron shielding ability evaluated for the barium doped lead phosphate glasses. Monte Caro code (MCNP-5) and the Phy-X/PSD program applied to estimate the mass attenuation coefficient of the studied glasses. The decrease in the PbO ratio has a negative effect on the MAC. The highest MAC decreased from 65.896 cm^2/g to 32.711 cm^2/g at 0.015 MeV for BPP0 and BPP7, respectively. The calculated values of EBF and EABF showed that replacement of PbO with BaO contents in the studied BPP glasses helps to reduce the number of photons accumulated inside the studied BPP glasses.

1. Introduction

Materials used for nuclear safety must-have sole characteristics such as a suitable transparent, non-corrosive, withstanding high stress, and non-toxic [1]. Wherefore, great attention was directed to the use of the glass materials as radiation shielding due to their superior functionality compared to traditional shielding materials such as concrete and polymer [2–4].

Recently, glass compositions have been utilized in a wide range of protons, alpha, and ionizing radiation absorption in X-ray examination rooms in hospitals and X-ray screening rooms in airports [5]. Consequently, more materials would synthesize and investigate their shielding potentials. The unique physical, thermal, mechanical, and optical properties of glass places them in a pivot position among materials that would be significant players in the quest to find novel shielding materials [6–9]. The reasons, as mentioned above, explain why many glasses suggested for their radiation shielding capability with exciting results. These include but not limited to, silicate-, borosilicate-, tellurite-based glass systems, etc., [10–16].

Phosphate-based glasses are characterized by noticeable features that make them more appropriate for several applications such as laser host matrices [17,18], optical devices [17–19], and glass-to-metal seals [18]. The addition of certain metal oxides such as Al_2O_3, Fe_2O_3, ZnO, Bi_2O_3, and PbO to P_2O_5 glasses improve their chemical durability [18,20,21]. These additives lead to an increase in the average bond strength and cross-link density within phosphate chains. Therefore, phosphate glasses are very favorable candidates for long term storage of high-level nuclear wastes [20,22,23]. Among various phosphate glass systems, the alkali free PbO−P_2O_5 glass systems are known to be more stable against devitrification and moisture resistant. In contrast to the conventional alkali/alkaline earth oxide modifiers, PbO has the ability to form stable glasses due to its dual role; one as the modifier [24,25] if Pb−O is ionic and the other as the glass former, if Pb−O is covalent.

From formal reports, lead oxide (PbO) plays as network modifier depending on its content [26], whereas barium oxide (BaO) is

* Corresponding author. Department of Nuclear Power Plants and Renewable Energy Sources, Ural Power Engineering Institute, Ural Federal University, 5 Sofia Kovalevskaya St., Yekaterinburg, Russia.
E-mail addresses: kmakhmud@urfu.ru, karemabdelazeem@yahoo.com (K.A. Mahmoud).

https://doi.org/10.1016/j.net.2021.06.005

considered as network modifier oxide in the glass structure [27,28]. Doweidar et al. [28,29] reported that in B_2O_3–PbO glass systems, the PbO plays as a modifier oxide up to 50 mol%, and above that content, it can form PbO_4 tetrahedra through sharing corners with PO_4 units. This trend leads to an increase in the cross-linking of the network via the formation of P–O–Pb linkages. On the other hand, Doweidar et al. [30] reported that the PbO_4 tetrahedra were formed with increment the content of PbO for more than 20 mol% in the glass composition. The role of PbO insertion on structure, physical, optical, and radiation shielding properties investigated via several authors [27–35].

In radiation shielding using shields, the emphasis is mostly placed on photons (gamma- and X rays) and neutrons because of their penetrating ability compared to other forms of ionizing radiation. Validation of the competency of any glass system to function as a shield must, therefore, include the study of shielding parameters of these radiations [31–36].

The objective of this work is to evaluate the mechanical properties of the lead phosphate doped BaO glasses. Furthermore, assess and analyze the ability of barium doped lead phosphate glasses to attenuate the incoming photons and fast neutrons.

2. Materials and methods

2.1. Mechanical properties

To achieve the objective of this study, eight glasses of barium doped lead phosphate glasses concerning the formula xBaO+(50-x) PbO+50P_2O_5, where x = 0–50 mol % were chosen from Ref. [36] as listed in Table 1. The density observed to decrease from 4.70 to 3.65 g cm^{-3}, with an increase in the BaO insertion ratio from 0 to 50 mol %. The main reason for reducing the glass density is the replacement of the PbO content with molecular weight (MW = 223.199 g/mol) by BaO with molecular weight (MW = 153.326 g/mol).

According to Makishima-Mackenzie's model, the elastic properties of BaO–PbO–P_2O_5 glasses evaluated at room temperature (298 K). The elastic moduli computed theoretically based on the values of the packing factor (V_i) and the heat of formation for each compound (dissociation energy, G_i, kJ/cm3) constituting the glass network [37,38], it is described by equation (1). Based on the calculated values of dissociation energy (G_t) and the packing density (V_t), elastic characteristics such as Young (Y), bulk (B), shear (S), and longitudinal (L) modulus calculated according to equations (3)–(6). Poisson ratio (μ) is a measure for the expansion generated in the material in a direction perpendicular to the compression direction, it can be described by equation (7). Moreover, the microhardness (H, GPa) is used to describe the hardness of the materials in micro scale when it is exposed to low applied loads. It can be described by equation (8).

$$G_t\ (kJ\ /\ cm) = \sum_i X_i\ G_i \tag{1}$$

$$V_t\ \left(cm^3\ \Big/\ mol\right) = \frac{\rho}{M}\sum_i X_i\ V_i \tag{2}$$

$$Y = 2V_tG \tag{3}$$

$$B = 1.2\ V_tE \tag{4}$$

$$S = \frac{3\ YB}{(9B - Y)} \tag{5}$$

$$L = B + \frac{3}{4}\ S \tag{6}$$

$$\mu = \frac{Y}{2\ S} - 1 \tag{7}$$

$$H = \frac{(1 - 2\mu)}{6(1 + \mu)} \tag{8}$$

$$T_g = \frac{M}{0.5074\ \rho\ v_s^2} \tag{9}$$

The G_i, V_i, and X_i represent the dissociation energy, packing factor, and molar fraction of the ith constituent compound in the glass network while ρ and M refer to the density and molecular weight of the studied glass.

2.2. Shielding parameters simulation

The average track length of gamma simulated for the barium doped lead phosphate (BPP) glasses using the Monte Carlo code (MCNP-5) at different gamma-photon energies. Accurate estimation of the average track length for ionizing radiation using MCNP required an input file. This input file should contain all necessary data about the geometry locations and constituents, the used sources (SDEF card), and composition (material card). In the present study, the geometry used for simulation is specified in Fig. 1 where all tools are set up according to the experimental facilities. A monoenergetic gamma-ray source located inside a collimator of lead with the highest 15 cm and diameter 7 cm and has a slit with a diameter of 1 cm. According to the present work, the samples molded in a disk form with a diameter of 5 cm. The studied samples placed at a distance of 10 cm from the radioactive source. Finally, the detector assumed to be F4 tally and located at a distance 10 cm far from the BPP glasses. The simulation was carried out using NPS card = 10^6 particles. The uncertainty recorded in the MCNP-5 code

Table 1
Chemical composition, density, molecular weight, and molar volume of xBaO+(50-x) PbO+50P_2O_5, x = 0,5, 10, 15, 20, 30, 40, 50 mol % glasses.

Sample code	Chemical composition (mol %)			Density (g cm^{-3})	Molecular weight (g mol^{-1})	Molecular volume (cm^3 mol^{-1})
	BaO	PbO	P_2O_5			
BPP0	0	50	50	4.70	182.57	38.85
BPP1	5	45	50	4.60	179.08	38.93
BPP2	10	40	50	4.50	175.58	39.02
BPP3	15	35	50	4.40	172.09	39.11
BPP4	20	30	50	4.30	168.60	39.21
BPP5	30	20	50	4.05	161.61	39.90
BPP6	40	10	50	3.85	154.62	40.16
BPP7	50	0	50	3.65	147.64	40.45

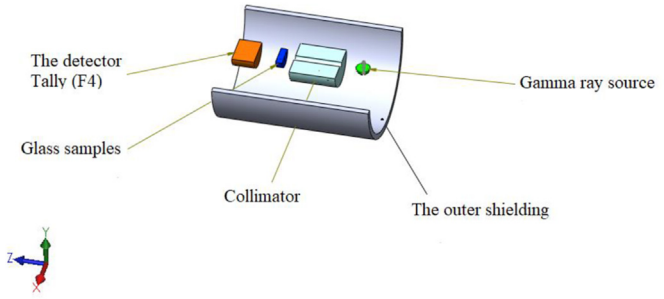

Fig. 1. The geometry used for simulation gamma ray shielding parameters [39–41].

output file varied around ± 1% [39–41].

After that, the estimated average track length used to calculate essential shielding parameters such as linear attenuation coefficient (LAC), mass attenuation coefficient (MAC), and others that can be estimated via Phy-X/PSD program [42].

3. Results and discussion

The present work deals with a study of the substitution effect of PbO by BaO contents on the mechanical properties of the investigated glasses. Wherefore, the elastic characteristics such as Young's, bulk, shear, and longitudinal modulus, Poisson ratio (μ), micro-hardness (H), and softening temperature (Ts) are calculated. The calculations based on the dissociation energy (G_i) and packing factor (V_i) for metal oxides constituting the investigated glass. Packing factor (V_i) and dissociation energy per unit volume (G_i, kJ cm^{-3}) are the basic units in the Makishima-Mackenzie theory. The computed data of G_t, V_i, and packing density (V_t) listed in Table 2. The variation of the calculated dissociation energy (G_t, kJ cm^{-3}), and packing factor (V_i, cm^3 mol^{-1}) versus the BaO content illustrated in Fig. 2. Fig. 2 depicts that the variation of the calculated dissociation energy (G_t, kJ cm^{-3}) versus the BaO content is completely opposite to the packing factor (V_i) of the investigated glasses. The dissociation energy for the investigated glasses found to increase in the range between 26.750 and 33.850 kJ cm^{-3} while the packing factor decreased from 23.250 to 21.900 cm^3 mol^{-1} with increasing the BaO between 0 and 50 mol %. This is due to the substitution of the PbO ($G_i = 25.3$ kJ cm^{-3} and $V_i = 11.7$ cm^3 mol^{-1}) with BaO ($G_i = 39.5$ kJ cm^{-3} and $V_i = 9$ cm^3 mol^{-1}) [43].

The elastic properties calculated according to Eqs (1)–(9) and listed in Table 2. Table 2 utilized that Young's model is directly proportional to the dissociation energy of investigated glasses. Wherefore, Young's modulus observed to increase with an increase in the BaO contents. The variation of Young's modulus versus the BaO insertion ratio illustrated in Fig. 3. In Fig. 3, Young's model increased in the range from 32.021 to 36.655 GPa. Eqs (4)–(6) depicts that bulk's, shear, and longitudinal modulus are based on and

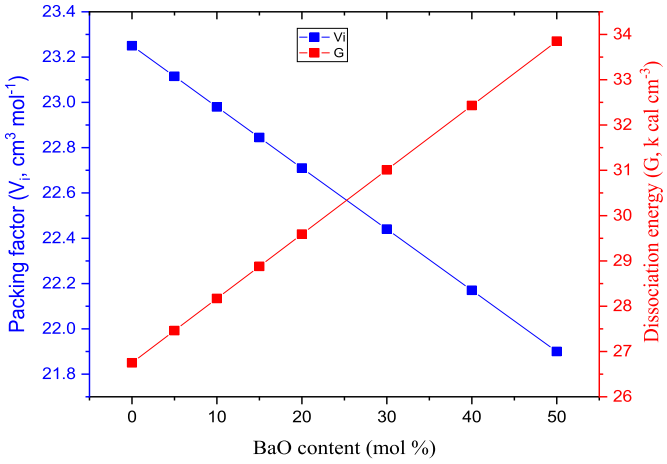

Fig. 2. The variation of packing density (V_i) and dissociation energy(G) of the studied glasses versus the BaO contents.

directly proportional to Young's modulus. Therefore, mechanical moduli (bulk, shear, and longitudinal) observed to increase with an increase in the BaO contents. This increase is due to the increase of the glasses's Gt form 26.750–33.850 kJ cm^{-3} and decreasing the packing density from 0.599 to 0.541 with the replacement of PbO with BaO content. Also, the detected increase mechanical moduli this is also related to replacement of Pb–O bonds with ($G_i = 25.3$ kJ cm^{-3} and $V_i = 11.7$ cm^3 mol^{-1}) by Ba–O bonds with ($G_i = 39.5$ kJ cm^{-3} and $V_i = 9$ cm^3 mol^{-1}). The straight lines in Fig. 3 showed the linear fitting of the calculated results where the values of R-square are 0991, 0.987, 0.995, and 0.959 for Young's, bulk, shear, and longitudinal modulus, respectively. Poisson ratio and the micro-hardness of the investigated glasses observed to have construct modes of variation with the BaO ratio see Fig. 4. Poisson ratio was found to decrease between 0.268–0.243, while the micro-hardness increased from 1.953 to 2.521 GPa with an increase in the BaO ratio from 0 to 50 mol%.

The predicted results were compared to some experimental results for two previously fabricated glasses like our BPP1 and BPP7 glasses, as listed in Table 2. The predicted mechanical moduli as well as the Poisson ratio, and micro-hardness for BPP1 and BPP7 glasses are comparable to the experimental results received for glasses 50P2O5–50PbO and 50P2O5–50ZnO that reported in Ref. [44]. In addition, softening temperature (T_g) used to describe the critical temperature where the glass transition occurred above this temperature. The variation of T_g versus the BaO content illustrated in Fig. 5. The calculated values of T_g observed to increase gradually with an increase in the BaO insertion ratio. T_g values increased from 205.682 to 321.900 °C. This increase in the T_g is due to the replacement of PbO (melting point = 888 °C) by BaO with a

Table 2
The mechanical properties of the investigated BPP0-BPP7 glasses.

Glass code	Mechanical properties									
	V_i (cm^3 mol^{-1})	G_t (kJ cm^{-3})	V_t (cm^3 mol^{-1})	E (GPa)	B (GPa)	S (GPa)	μ	H (GPa)	L (GPa)	Softening temperature (°C)
BPP0	23.250	26.750	0.599	32.021	22.999	12.627	0.268	1.953	39.835	205.682
BPP1	23.115	27.460	0.594	32.609	23.234	12.878	0.266	2.008	40.405	214.795
BPP2	22.980	28.170	0.589	33.181	23.450	13.124	0.264	2.063	40.949	224.268
BPP3	22.845	28.880	0.584	33.737	23.647	13.364	0.262	2.119	41.466	234.127
BPP4	22.710	29.590	0.579	34.278	23.825	13.600	0.260	2.174	41.958	244.400
BPP5	22.440	31.010	0.562	34.877	23.536	13.917	0.253	2.291	42.092	270.247
BPP6	22.170	32.430	0.552	35.804	23.717	14.340	0.248	2.405	42.837	294.814
BPP7	21.900	33.850	0.541	36.655	23.816	14.739	0.243	2.521	43.468	321.900

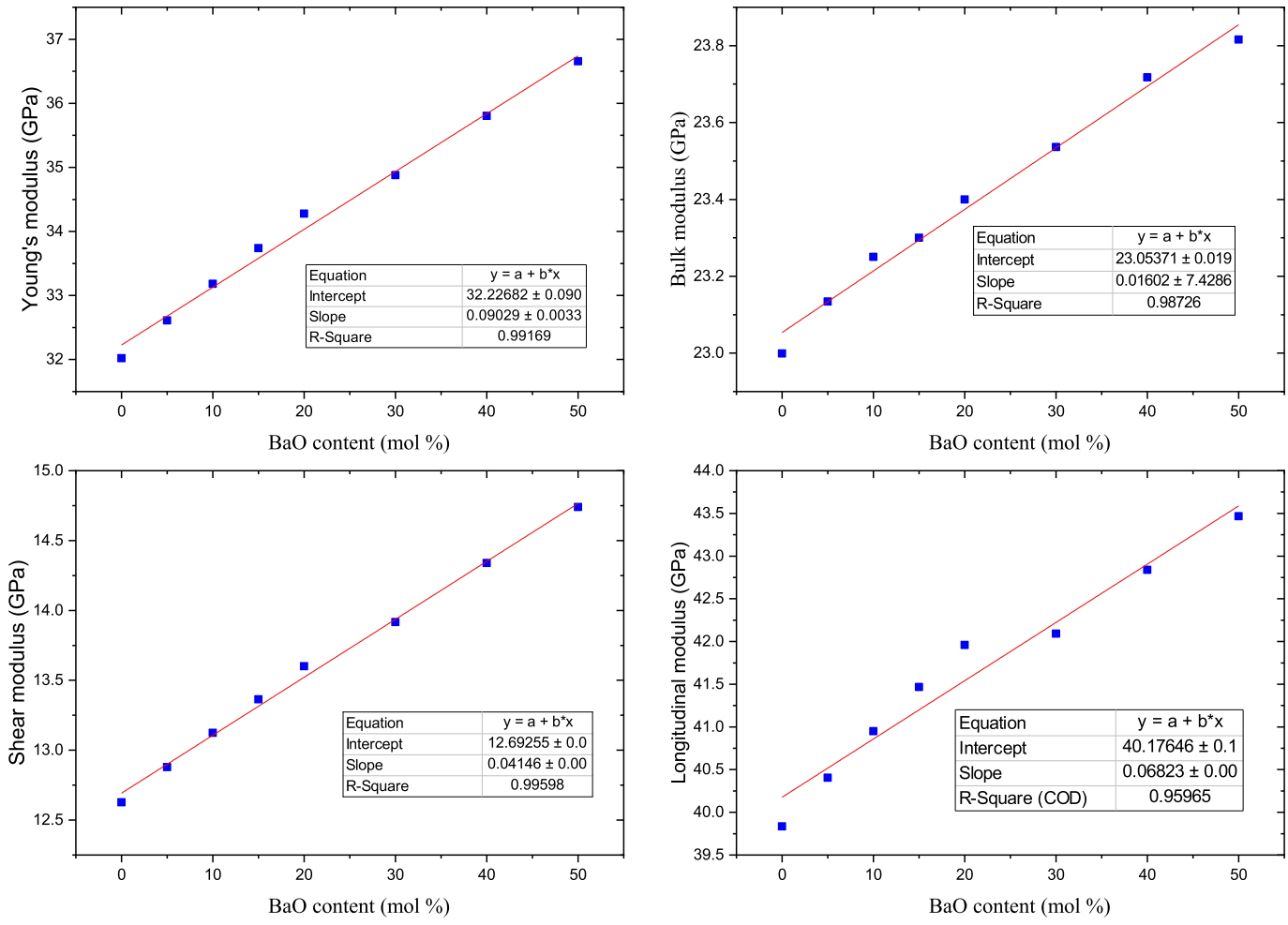

Fig. 3. The variation of the mechanical module (Young, bulk, Shear, and Longitudinal) versus the BaO contents.

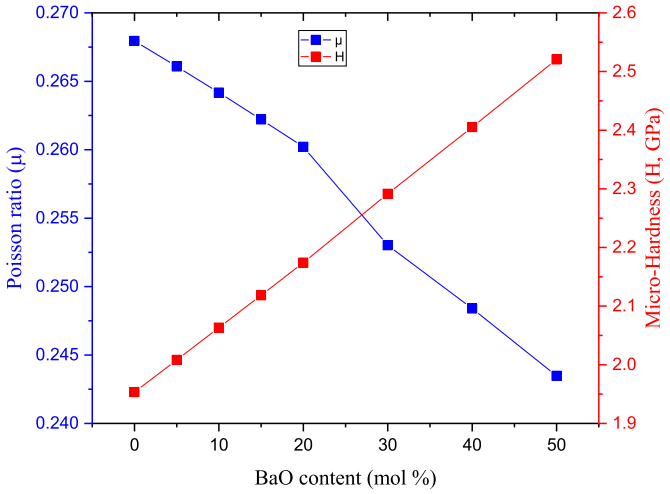

Fig. 4. Variation of the Poisson ratio and the microhardness of as a function of the BaO content in the studied glasses.

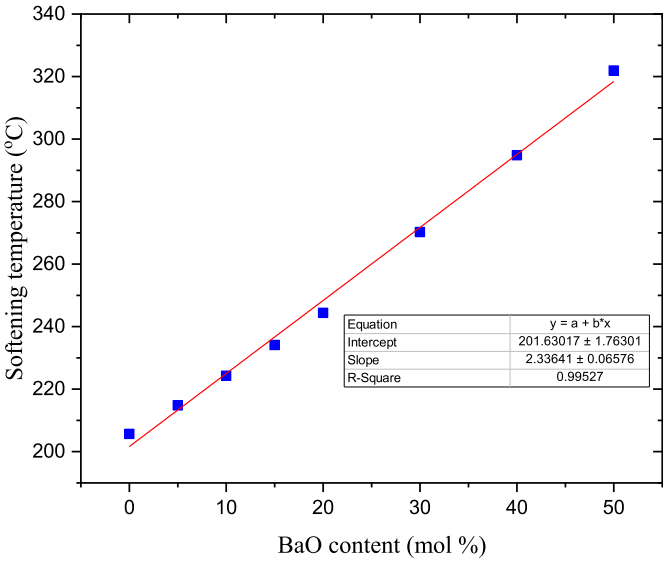

Fig. 5. Changing of the softening temperature as a function of the BaO content in the studied glasses.

higher melting point (melting point = 1923 °C).

To examine the shielding capacity of the investigated glasses, the mass attenuation coefficient (MAC) has been evaluated. Phy-X/PSD program and MCNP-5 code are two different methods used to estimate the MAC. Fig. 6 introduces the simulated and theoretically calculated MAC versus the photon energy in the range 0.015–15 MeV. It is more evident from the two figures that the MAC

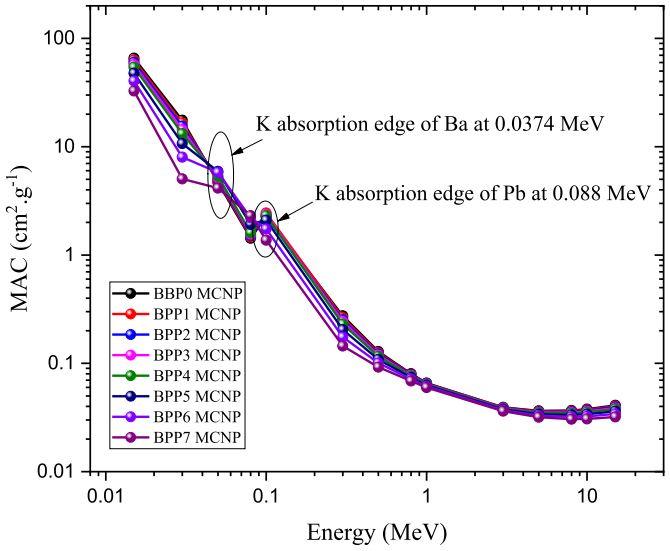

Fig. 6. The MAC of barium doped lead phosphate (BPP4-BPP7) glasses versus gamma photons energy.

acquires the highest values at the very low energy photons. After that, the obtained MAC values decreased sharply with an increase in the photon energy up to 0.1 MeV, where the photoelectric interaction probabilities decreased with increasing the photons energy in this region and vary with $Z^4/E^{3.5}$. During the interaction all photon energy is consumed to eject one boundary photon and the photon annihilated inside the glass layers. Thus, the attenuation capacity is higher in the PE interaction region. From 0.1 up to 3 MeV, the MAC has a quiet variation with photon energy. This is due to Compton scattering. Besides, the MAC has a minimal change with the incoming photon energy at gamma photon energy range from 3 up to 15 MeV because of the pair production interaction in this zone.

To study the effect of replacement of PbO by BaO contents on the shielding capacity of the glasses, one found that the decrease in the PbO ratio has a negative effect on the MAC values that decreased from 65.896 cm^2/g to 32.711 cm^2/g at 0.015 MeV for BPP0 and BPP7, respectively. At 15 MeV, the MAC values decreased from 0.041 cm^2/g to 0.032 cm^2/g for BPP0 and BPP7, respectively. These results assured the fact that the replacement of PbO with high atomic weight containing heavy element; (Pb, Z = 82) with a high ratio with an element with another oxide with atomic number less than PbO as the BaO that contains (Ba element, Z = 56) weakens the shielding capacity of the glasses under study. It illustrated in Figs. 2 and 3 that within the decrease of the MAC values in the low energy photons, one noted an increase in one or two positions according to the K-absorption edges of elements forming the composition of the glasses (Pb and Ba). In Fig. 6, one found only a characteristic and sharp peak at 0.088 MeV related to Pb with the highest weight fraction ratio 0.5674 while no peak found related to Ba because of this sample free of barium. The peak associated with Pb gradually decreased till it vanished at BPP7 that is free of lead, on the other hand, an increase in MAC found at 0.0374 MeV (tiny peak) associated with Ba in the glass composition. This peak began to increase till reaching its maximum position at BPP7 that characterized the highest weight fraction of Ba is 0.4651. The obtained data from theoretical and simulation methods presented in Tables S1, the relative deviation calculated, and the results matched each other. Finally, we find the MAC values exhibit the order that $(MAC)_{BPP0} > (MAC)_{BPP1} > (MAC)_{BPP2} > (MAC)_{BPP3} > (MAC)_{BPP4} > (MAC)_{BPP5} > (MAC)_{BPP6} > (MAC)_{BPP7}$. These results introduced BPP0 as a superior candidate to shield against gamma radiation among all BPP glasses.

Half value layer is a parameter that presents the desired material thickness needed to attenuate half of the incident photons and is plotted in Fig. 7 for the BPP glasses. The HVL is inversely proportional to the LAC of the studied glasses. Thus, the thinner values of the HVL achieved at low gamma-photon energy. After that, the HVL increased gradually with increasing photon energy. Glass coded BPP7 has the highest HVL value varied in the range of 0.006–5.927 cm at gamma-photon energy varied in the range between 0.015 and 15 MeV. On the other hand, glass coded BPP0 has the lowest HVL values and changes between 0.002 and 3.595 cm at gamma photon energy between 0.015 and 15 MeV, respectively. It is worth noting that BPP compared with two commercial materials, namely RS-253-G18 and RS 360. Results reveal that most of the selected BPP glasses have better gamma-ray shielding capacity than RS-253-G18, while all BPP glasses have better shielding capacity than RS 360.

Dependence of the effective atomic number (Z_{eff}) of BPP0–BPP7 glasses on photon energy depicted in Fig. 8. The highest Z_{eff} obtained for BPP0 and varied in the range between 67.76–32.25 while the lowest achieved for glass BPP7 and changed from 42.21 to 21.88. The behavior of the Z_{eff} can be similarly discussed as mass attenuation coefficient trend with photon energy according to the interaction mechanism of photons with matter. Furthermore, the sample with higher MAC (BPP0) has also the highest Z_{eff}.

Moreover, the software program Phy-X/PSD was applied to calculate the buildup factors EBF and EABF (exposure buildup factor and energy absorption buildup factor respectively) for the studied BPP glasses at various penetration depth (PD) and gamma photon energy (E) [42]. The obtained EBF and EABF results for the studied BPP glasses were plotted against the incoming gamma photon energy and the barium concentration, as presented in Fig. 9. According to these figures, two essential points should be discussed. The first point is the variation of EBF and EABF values versus the incoming gamma photon energy. The lowest EBF and EABF values detected for low photon energy, where the photoelectric interaction (PE) is the dominant gamma photon interaction. The incoming photon energy is totally absorbed by the boundary electron in the studied glasses. Thus, the photons absorbed in the studied glasses and prevented from accumulating. In the PE interaction region, there two increases in the values of EBF and EABF were detected

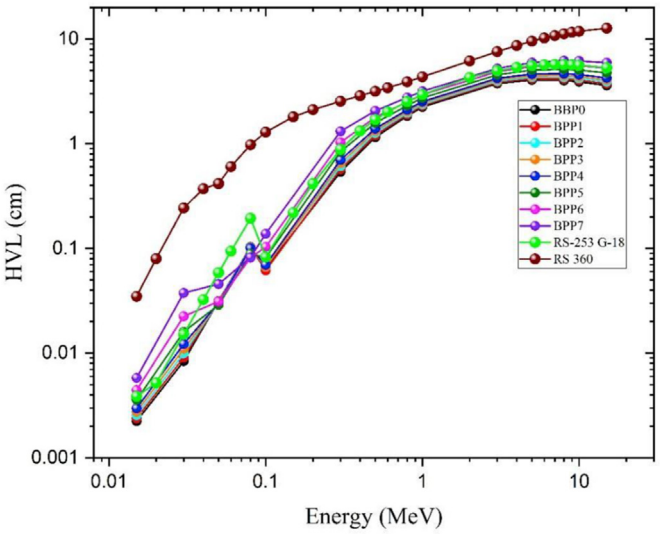

Fig. 7. The HVL of barium doped lead phosphate (BPP0-BPP7), RS 253-G18 and Rs-360 shielding glasses versus gamma photons energy.

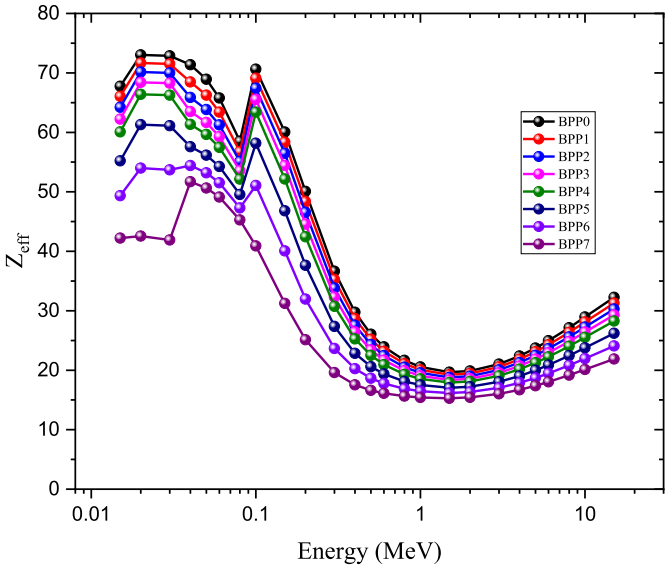

Fig. 8. The Z_{eff} of barium doped lead phosphate (BPP0-BPP7) glasses versus gamma ray photon energies.

around 0.04 and 0.09 MeV. The first increase is due to the X-ray absorption K-edges of Ba, while the second is due to the absorption K-edges of Pb. The amplitude of the K-absorption peaks for Ba and Pb are directly proportional to the ratios of their compounds (BaO and PbO) in the studied BPP glasses. Above 0.1 MeV, the Compton scattering interaction (CS) began to increase and reached the maximum around 1 MeV. Thus, the calculated values of EBF and EABF were progressively increasing with the increase of the incoming gamma photon energy. The gradual increases in the EBF, and EABF values are due to the accumulation of incoming photons inside the studied BPP glasses. During the Compton scattering process, only a part of the incoming photon energy is removed to eject a boundary electron. Above 1.5 MeV, the calculated values of the buildup factors were slowly reduced again due to the pair production interaction (PP). During the PP interaction, the energy of incoming photons consumed to produce an electron-positron pair. Above 8 MeV, a rapid increase in the EBF and EABF values was detected, especially at high penetration depth (PD > 20). The second point is the variation of the buildup factors is the BaO contents. The calculated values of EBF and EABF showed that replacement of PbO with BaO contents in the studied BPP glasses helps to reduce the number of photons accumulated inside the studied BPP glasses. In order to assume a good suitable shielding material, they should have both suitable shielding capacity and hardness. Thus, the variation of the glasses' microhardness and the LAC (shielding capacity) versus the BaO ratio inserted to the glass was illustrated in Fig. 10. The investigated glasses LAC increases while the micro-hardness decreases with increasing the BaO insertion ratio. The best shielding capacity achieved for glasses without BaO concentration (i.e., BPP1) while the best hardness achieved for glasses with BaO of 50 mol% (i.e., BPP7) while the lowest achieved for glasses without BaO contents (i.e., BPP1). As shown in Fig. 11, the best glass samples which have a suitable shielding and mechanical materials are that have BaO content around 25 and 30 mol%. These glasses have linear attenuation coefficient around 0.465 cm-1 at 0.5 MeV, and their micro-hardness 2.25 GPa.

The calculated effective removal cross-section $\sum_R$ ($cm^2\ g^{-1}$) of the fast neutrons for the studied BPP0-BPP7 glasses plotted in Fig. 11. The $\sum_R$ observed to increase gradually with increase BaO

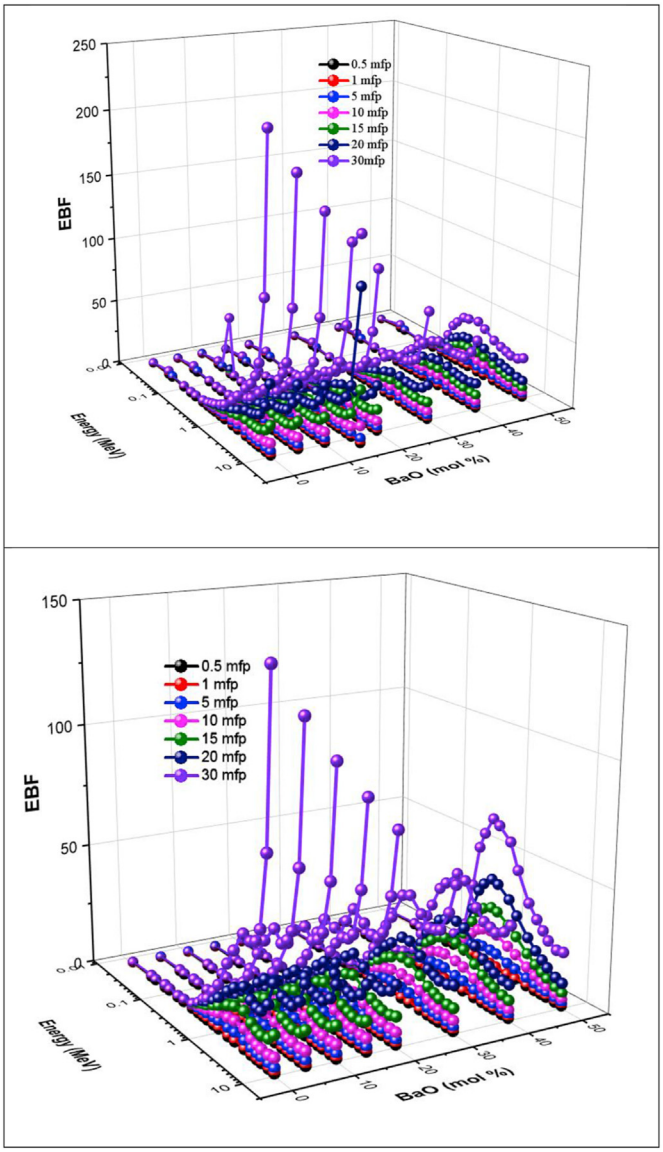

Fig. 9. The exposure and energy absorption buildup factors (EBF and EABF) of barium doped lead phosphate glasses (BPP0-BPP3) versus gamma photons energy.

contents on the studied BPP glasses. This increase may be due to the replacement of PbO, which has a higher density (9.53 g cm^{-3}) and molar mass (223.2 g mol^{-1}) with BaO, which has a lower density (5.72 g cm^{-3}) and molar mass (153.33 g mol^{-1}). The smallest fast neutron effective removal cross-section is equaling 0.0211 $cm^2\ g^{-1}$ and obtained for the studied glass BPP0 while the highest effective removal cross-section is equaling 0.0248 $cm^2\ g^{-1}$) and received by the studied glasses BPP7.

4. Conclusion

In this article, the mechanical properties of the barium doped lead phosphate glasses evaluated using Makishima-Mackenzie's model. The elastic moduli, such as Young, bulk, shear, and longitudinal, enhanced with the replacement of the PbO by BaO contents. Also, the micro-hardness and softening temperature increase with an increase in the ratio of BaO in the investigated glass. Furthermore, the radiation shielding properties for gamma - photons and fast neutrons analyzed and evaluated. Results revealed

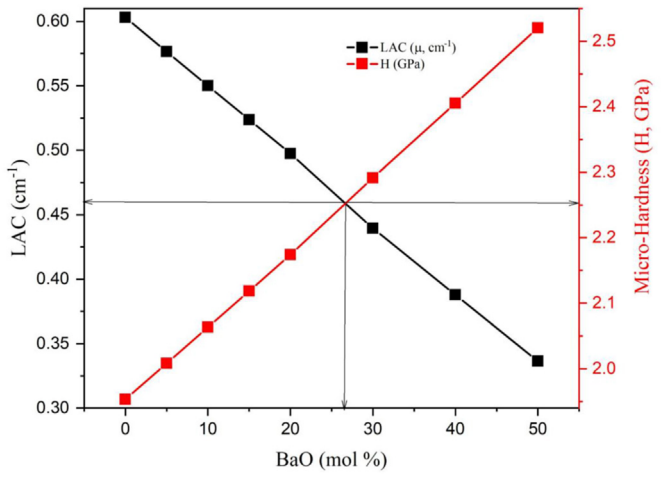

Fig. 10. Assess of the fabricated glass' attenuation capacity and the mechanical properties.

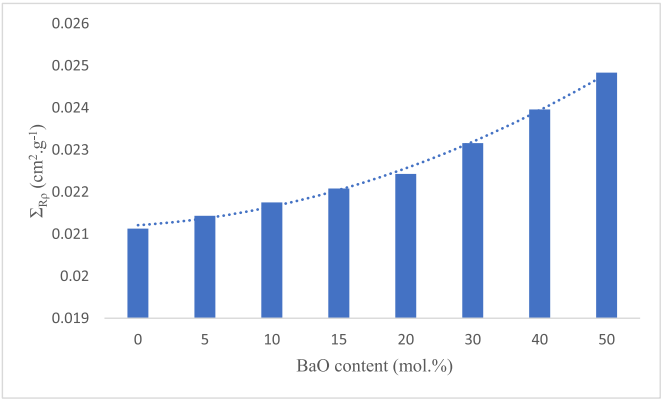

Fig. 11. The effective removal cross section of fast neutrons Σ_R for barium doped lead phosphate glasses.

that the decrease in the PbO ratio has a negative effect on the MAC values. Besides, in terms of HVL, the BPP7 glass sample has the highest value while BPP0 has the lowest value. Furthermore, the calculated values of EBF and EABF showed that replacement of PbO with BaO contents in the studied BPP glasses helps to reduce the number of photons accumulated inside the studied BPP glasses. Finally, the lowest fast neutron effective removal cross equaling ($\sum_R = 0.0211$ cm^2 g^{-1}) and obtained for the studied glass BPP0 while the highest effective removal cross-section equaling 0.0248 cm^2 g^{-1} and received for the studied glasses BPP7.

Declaration of competing interest

The authors declare that they have no known competing financial interests or personal relationships that could have appeared to influence the work reported in this paper.

Acknowledgment

Taif University, Saudi Arabia is kindly acknowledged for Supporting our work through the Project number (TURSP-2020/84).

Appendix A. Supplementary data

Supplementary data to this article can be found online at https://doi.org/10.1016/j.net.2021.06.005.

References

[1] S.A.M. Issa, T.A. Hamdalla, A.A.A. Darwish, Effect of $ErCl_3$ in gamma and neutron parameters for different concentration of $ErCl_3$-SiO_2 (EDFA) for the signal protection from nuclear radiation, J. Alloys Compd. 698 (2017) 234–240.
[2] D.K. Gaikwad, S.S. Obaid, M.I. Sayyed, R.R. Bhosale, V.V. Awasarmol, A. Kumar, M.D. Shirsat, P.P. Pawar, Comparative study of gamma ray shielding competence of WO_3-TeO_2-PbO glass system to different glasses and concretes, Mater. Chem. Phys. 213 (2018) 508–517.
[3] Y.S. Rammah, F.I. El-Agawany, K.A. Mahmoud, R. El-Mallawany, Ilik Erkan, Kilic Gokhan, FTIR, UV–Vis–NIR spectroscopy, and gamma rays shielding competence of novel ZnO-doped vanadium borophosphate glasses, J. Mater. Sci. Mater. Electron. 31 (2020) 9099–9113, https://doi.org/10.1007/s10854-020-03440-5.
[4] V.P. Singh, H.O. Tekin, N.M. Badiger, T. Manici, E.E. Altunsoy, Effect of heat treatment on radiation shielding properties of concretes, Journal of Radiation Protection and Research 43 (1) (2018) 20–28, https://doi.org/10.14407/jrpr.2018.43.1.20.
[5] Y.S. Rammah, Influence of Ag_2O insertion on alpha, proton and γ-rays safety features of TeO_2.ZnO.Na_2O glasses: potential use for nuclear medicine applications, Ceram. Int. 46 (11Part A) (2020) 18151–18159, https://doi.org/10.1016/j.ceramint.2020.04.136.
[6] C. Bootjomchai, J. Laopaiboon, C. Yenchai, R. Laopaiboon, Gamma-ray shielding and structural properties of barium-bismuth-borosilicate glasses, Radiat. Phys. Chem. 81 (2012) 785–790, https://doi.org/10.1016/j.radphyschem.2012.01.049.
[7] A.A.A. Darwish, S.A.M. Issa, M.M. El-Nahass, Efect of gamma irradiation on structural, electrical and optical properties of nanostructure thin flms of nickel phthalocyanine, Synth. Methods 215 (2016) 200–206, https://doi.org/10.1016/j.synthmet.2016.03.002.
[8] B.O. Elbashir, M.G. Dong, M.I. Sayyed, S.A.M. Issa, K.A. Matori, M.H.M. Zaid, Comparison of Monte Carlo simulation of gamma-ray attenuation coefficients of amino acids with XCOM program and experimental data, Results Phys 9 (2018) 6–11, https://doi.org/10.1016/j.rinp.2018.01.075.
[9] S.A.M. Issa, Y.B. Saddeek, H.O. Tekin, M.I. Sayyed, K. Saber Shaaban, Investigations of radiation shielding using Monte Carlo method and elastic properties of PbO-SiO2-B2O3-Na2O glasses, Curr. Appl. Phys. 18 (2018) 717–727.
[10] S.A.M. Issa, M.I. Sayyed, M.H.M. Zaid, K.A. Matori, Photon parameters for gamma-rays sensing properties of some oxide of lanthanides, Results Phys 9 (2018) 206–210, https://doi.org/10.1016/j.rinp.2018.02.039.
[11] R. Mirji, B. Lobo, Computation of the mass attenuation coefficient of polymeric materials at specifc gamma photon energies, Phys.Chem. Radiat. 1 (2017) 1, https://doi.org/10.1016/j.radphyschem.2017.03.001.
[12] M.I. Sayyed, S.A.M. Issa, S.H. Auda, Assessment of radio-protective properties of some anti-infammatory drugs, Prog. Nucl. Energy 100 (2017) 297–308, https://doi.org/10.1016/j.pnucene.2017.07.003.
[13] K.J. Singh, S. Kaur, R.S. Kaundal, Comparative Study of Gammaray Shielding and Some.
[14] A.A. Ali, Y.S. Rammah, M.H. Shaaban, The influence of TiO_2 on structural, physical and optical properties of B_2O_3 –TeO_2 – Na_2O – CaO glasses, J. Non-Cryst. Solids 514 (2019) 52–59.
[15] Y.S. Rammah, Gökhan Kilic, R. El-Mallawany, U. Gökhan Issever, F.I. El-Agawany, Investigation of optical, physical, and gamma-ray shielding features of novel vanadyl boro-phosphate glasses, J. Non-Cryst. Solids 533 (2020), 119905.
[16] Y.S. Rammah, F.I. El-Agwany, K.A. Mahmoud, A. Novatski, R. El-Mallawany, Role of ZnO on TeO_2. Li_2O. ZnO glasses for optical and nuclear radiation shielding applications utilizing MCNP5 simulations and WINXCOM program, J. Non-Cryst. Solids 544 (2020), 120162.
[17] G. Moulika, S. Sailaja, B.N.K. Reddy, V.S. Reddy, S. Dhoble, B.S. Reddy, Optical properties of Eu^{3+} & Tb^{3+} ions doped alkali oxide (Li_2O/Na_2O/K_2O) modified boro phosphate glasses for red, green lasers and display device applications, Physica B 535 (2018) 2–7.
[18] M.K. Hwang, I.G. Kim, B.K. Ryu, Study of water resistance of Fe_2O_3 doped P_2O_5–ZnO–Bi_2O_3 sealing glass system, Korean J. Met. Mater. 54 (2016) 621–625.
[19] M. Saad, H. Elhouichet, Good optical performances of Eu^{3+}/Dy^{3+}/Ag nanoparticles co-doped phosphate glasses induced by plasmonic effects, J. Alloys Compd. 806 (2019) 1403–1409.
[20] J.-H. Hsu, J. Bai, C.-W. Kim, R.K. Brow, J. Szabo, A. Zervos, The effects of crystallization and residual glass on the chemical durability of iron phosphate waste forms containing 40 wt% of a high MoO_3 Collins-CLT waste, J. Nucl. Mater. 500 (2018) 373–380.
[21] F.Z. Souissi, H. Ettoumi, M. Barré, M. Toumi, Preparation and electrical conductivity of potassium phosphate glasses containing Al_2O_3, J. Non-Cryst. Solids 481 (2018) 585–589.
[22] P. Pascuta, G. Borodi, N. Jumate, I. Vida-Simiti, D. Viorel, E. Culea, The structural role of manganese ions in some zinc phosphate glasses and glass ceramics, J. Alloys Compd. 504 (2010) 479–483.
[23] Y. Lai, X. Liang, G. Yin, S. Yang, J. Wang, H. Zhu, H. Yu, Infrared spectra of iron

phosphate glasses with gadolinium oxide, J. Mol. Struct. 1004 (2011) 188–192.
[24] G. Cormier, J.A. Capobianco, A. Monteil, Molecular dynamics simulation of lead metaphosphate $Pb(PO_3)_2$ glass, J. Non-Cryst. Solids 168 (1994) 115–124.
[25] G. Little Flower, G. Sahaya Baskaran, M. Srinivasa Reddy, N. Veeraiah, The structural investigations of $PbO-P_2O_5-Sb_2O_3$ glasses with MoO3 as additive by means of dielectric, spectroscopic and magnetic studies, Physica B 393 (2007) 61–72.
[26] C. Dayanand, G. Bhikshamaiah, V.J. Tyagaraju, M. Salagram, A.S.R. Krishna Murthy, Structural investigations of phosphate glasses: a detailed infrared study of the x(PbO)-(1–x) P_2O_5 vitreous system, J. Mater. Sci. 31 (1996) 1945–1967.
[27] C. Ivascu, A. Timar Gabor, O. Cozar, L. Daraban, I. Ardelean, FT-IR, Raman and thermoluminescence investigation of $P_2O_5-BaO-Li_2O$ glass system, J. Mol. Struct. 993 (2011) 249–253.
[28] H. Doweidar, G. El-Damrawi, E. El Agammy, Structural correlations in BaO–PbO–B2O3 glasses as inferred from FTIR spectra, Vib. Spectrosc. 73 (2014) 90–96.
[29] H. Doweidar, K. El-Egili, R. Ramadan, M. Al-Zaibani, Structural investigation and properties of $Sb_2O_3-PbO-B_2O_3$ glasses, J. Non-Cryst. Solids 497 (2018) 93–101.
[30] H. Doweidar, A.H. Oraby, Density of lead borate glasses in relation to the microstructure, Phys. Chem. Glasses 38 (1997) 69–73.
[31] Y.S. Rammah, K.A. Mahmoud, E. Kavaz, Ashok Kumar, F.I. El-Agawany, The role of PbO/Bi_2O_3 insertion on the shielding characteristics of novel borate glasses, Ceram. Int. (2020), https://doi.org/10.1016/j.ceramint.2020.04.018.
[32] Y.S. Rammah, K.A. Mahmoud, M.I. Sayyed d, F.I. El-Agawany, R. El-Mallawany, Novel vanadyl lead-phosphate glasses: $P_2O_5-PbO-ZnO-Na_2O-V_2O_5$: synthesis, optical, physical and gamma photon attenuation properties, J. Non-Cryst. Solids 534 (2020), 119944.
[33] U. Perişanoğlu, F.I. El-Agawany, E. Kavaz, M. Al-Buriahi, Y.S. Rammah, Surveying of $Na_2O_3-BaO-PbO-Nb_2O_5-SiO_2-Al_2O_3$ glass-ceramics system in terms of alpha, proton,neutron and gamma protection features by utilizing GEANT4 simulation codes, Ceram. Int. 46 (2020) 3190–3202.
[34] M.S. Al-Buriahi, F.I. El-Agawany, C. Sriwunkum, Hakan Akyıldırım, Halil Arslan, B.T. Tonguc, R. El-Mallawany, Y.S. Rammah, Influence of Bi_2O_3/PbO on nuclear shielding characteristics of lead-zinc-tellurite glasses, Physica B 581 (2020), 411946.
[35] Y. Al-Hadeethi, M.I. Sayyed, Y.S. Rammah, Fabrication, optical, structural and gamma radiation shielding characterizations of GeO_2-PbO-Al_2O_3–CaO glasses, Ceram. Int. 46 (2020) 2055–2062.
[36] M. Hamed Misbah, H. Doweidar, K. El-Egili, G. El-Damrawi, M. El-Kemary, Structure and some properties of $xBaO\cdot(50-x)PbO\cdot 50P_2O_5$ glasses, J. Non-Cryst. Solids 534 (2020), 119945.
[37] A. Makishima, J.D. Mackenzie, Direct calculation of Young's modulus of glass, J. Non-Cryst. Solids 12 (1973) 35–45.
[38] A. Makishima, J.D. Mackenzie, Calculation of Bulks modulus, Shear modulus and Piosson's ratio of glass, J. Non-Cryst. Solids 17 (1975) 147–157.
[39] R. Kurtulus, T. Kavas, K.A. Mahmoud, I. Akkurt, K. Gunoglu, M.I. Sayyed, The effect of Nb_2O_5 on waste soda-lime glass in gamma-rays shielding applications, J. Mater. Sci. Mater. Electron. 32 (4) (2021) 4903–4915, https://doi.org/10.1007/s10854-020-05230-5.
[40] Qiuling Chen, K.A. Naseer, K. Marimuthu, P. Suthanthira Kumar, Baoji Miao, K.A. Mahmoud, M.I. Sayyed, Influence of modifier-oxide on the structural and radiation shielding features of Sm^{3+} doped calcium telluro-fluoroborate glass system, Journal of the Australian Ceramics Society 57 (1) (2021) 275–286, https://doi.org/10.1007/s41779-020-00531-8.
[41] Y.S. Rammah, K.A. Mahmoud, F.I. El-Agawany, O.L. Tashlykov, E. Yousef, Tm^{3+} ions doped phosphate glasses: nuclear shielding competence and elastic moduli, Appl. Phys. A 126 (2020) 927, https://doi.org/10.1007/s00339-020-04109-w.
[42] E. Şakar, Ö.F. Özpolat, B. Alım, M.I. Sayyed, M. Kurudirek, Phy-X/PSD: development of a user friendly online software for calculation of parameters relevant to radiation shielding and dosimetry, Radiat. Phys. Chem. 166 (2020), 108496.
[43] S. Inaba, S. Fujino, K. Morinaga, Young's modulus and compositional parameters of oxide glasses, J. Am. Ceram. Soc. 82 (1999) 3501–3507.
[44] H.A.A. Sidek, R. El-Mallawany, K.A. Matori, M.K. Halimah, Effect of PbO on the elastic behavior of ZnO–P2O5 glass systems, Results in Physics 6 (2016) 449–455.